# Separating the Material and Geometry Contribution to the Circular Dichroism of Chiral Objects Made from Chiral Media

Lukas Rebholz,* Marjan Krstić, Benedikt Zerulla, Mateusz Pawlak, Wiktor Lewandowski, Ivan Fernandez-Corbaton, and Carsten Rockstuhl

ABSTRACT: The chirality of an object can be studied by measuring the circular dichroism, that is, the difference in absorption of light with different helicity. The chiral optical response of an object, however, can have two different origins. On the one hand, it can be linked to the chiral geometry of the object. On the other hand, it can be linked to the chiral material from which the object is made. Whereas previously no distinction between the two contributions could be made, we report here a computational approach that allows us to separate these two contributions to the circular dichroism of an object. We consider separately the case where geometry-related resonances affect the optical response and the case where they are absent. In both cases, we find the circular dichroism to be easily decomposable if a

geometrically achiral object has an absorption spectrum similar to that of the chiral object under investigation. Furthermore, in the nonresonant case, the contribution attributed to the material can be obtained without taking any geometry into account. Besides being of fundamental importance, the possibility of disentangling both contributions will be important for guiding the future design of chiral objects and devices.

KEYWORDS: circular dichroism, chirality, light−matter interaction, multiscale modeling, time-dependent density functional theory, finite element method
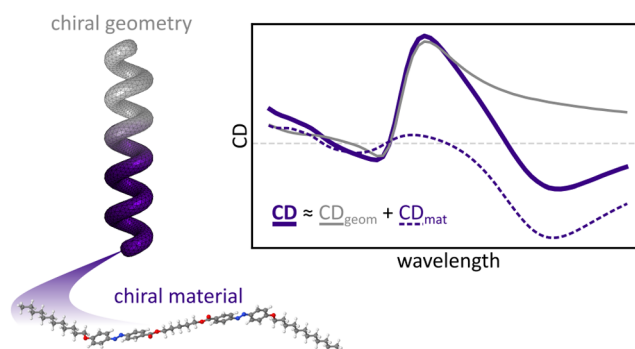
INTRODUCTION

Chiral objects exhibit a chiral optical response, i.e., they interact differently with light of different helicity.[1−3] An instance of such a phenomenon is circular dichroism (CD), which describes the difference in absorption depending on the helicity of the illumination.[4,5] CD can be utilized to probe the chirality of a given object spectroscopically. As such, CD is at the heart of multiple applications, ranging from sensing[6−10] and imaging[11,12] to quantum devices.[13] To infer the properties of the examined object from such measurements, understanding the relation between CD and the chirality of the object is crucial.[14,15]

For an object made from a homogeneous medium, two different causes can contribute to the chiral response. First, the chiral response can be due to the object's geometry.[16,17] A chiral response emerges if the geometry lacks mirror or inversion symmetry. This complies with the notion that a chiral object is not superimposable onto its mirror image. The second cause of chirality can be found in the properties of the medium from which the object is made.[18,19] In describing a homogeneous medium, this effect is captured by an ascribed chirality parameter in the constitutive relations representing the medium.[20] Examining such a material description in detail,

the cause for this material-related chirality can be understood in the same geometrical sense as that before. In this case, it is the molecules or the material constituents themselves that break the mirror and inversion symmetry.[21] Differentiating between these two origins of chirality is a distinction concerning the length scales on which chirality resides.

For an object having both origins of chirality, these two effects always cause the overall CD. An example of such an object is shown in Figure 1. The object in the shape of a helix is geometrically chiral, which can be characterized by a handedness that describes its twist.[22−24] Additionally, the object is made from a material characterized by chiral constitutive relations. In this specific case, the material is supposed to be organic and made from chiral molecules.[25,26] For such a system, the question arises as to whether the CD can be dissected regarding the two origins.
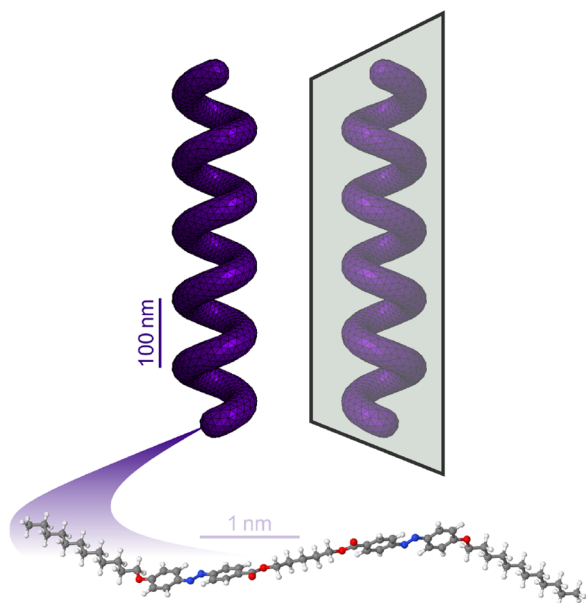
Figure 1. Representation of an object featuring chirality via its geometric shape and material properties. The helix can be characterized by a handedness following its twist direction. Since this handedness flips upon reflection, the right-handed original helix cannot be superimposed with its left-handed mirror image. Therefore, the helix is geometrically chiral. Additionally, the helix is made from a material consisting of organic molecules that themselves are chiral. The helix, thereby, combines the geometry-related chirality with the chirality of its molecular building blocks.

The relevance of understanding such systems becomes apparent when considering chiral organic materials that are often used for practical applications,[27] with the prominent examples of electroluminescent polymers,[28] chiral gels,[29] and morphologically chiral liquid crystals.[30] It is important to note that these materials may exhibit chirality across a range of length scales, from single molecule to supramolecular levels.

Thus, beyond considering the molecular architecture of single molecules, thin films of these substances should be considered as made of elements with characteristic sizes comparable to the visible light wavelength. The precise understanding of the origin of chiroptical properties in such systems is a complex challenge.[31]

Besides being of fundamental intellectual interest, separating chiral properties into individual contributions attributable to the two different scales of chirality could be of practical use, as well. For example, the numerical analysis of chiral objects could be simplified by analyzing these contributions independently,[32] choosing different, well-suited methods correspondingly. Moreover, the design of chiral objects made from a chiral material could consider both contributions as independent degrees of freedom.[33] This would allow us to tailor chiral optical responses and widen our range of accessible dispersive chiral properties.

In the following, a computational approach is presented to explore and understand the origin of CD of a chiral object made from a chiral molecular material. For that purpose, we combine quantum-chemical simulations,[34] capturing the properties of the chiral molecular material, with optical full-wave simulations,[35] capturing the optical response of the chiral object made from that chiral material. It is shown that the total CD can be written as a linear superposition of two contributions, each of them linked to one of the two origins: geometrical chirality and material chirality, respectively. The helix shown in Figure 1 is studied as a system in which no significant optical resonances are supported. In this case, the separation is particularly clean. Afterward, the importance of resonances is considered in studying a tetrahedral arrangement of resonant spheres. We use this to show that the distinction between the contributions remains feasible in systems where a geometrically chiral and an achiral object offer a similar optical response. This holds true in both resonant and nonresonant cases.

This Article is structured as follows: First, we sketch our multiscale approach to model the optical properties of an
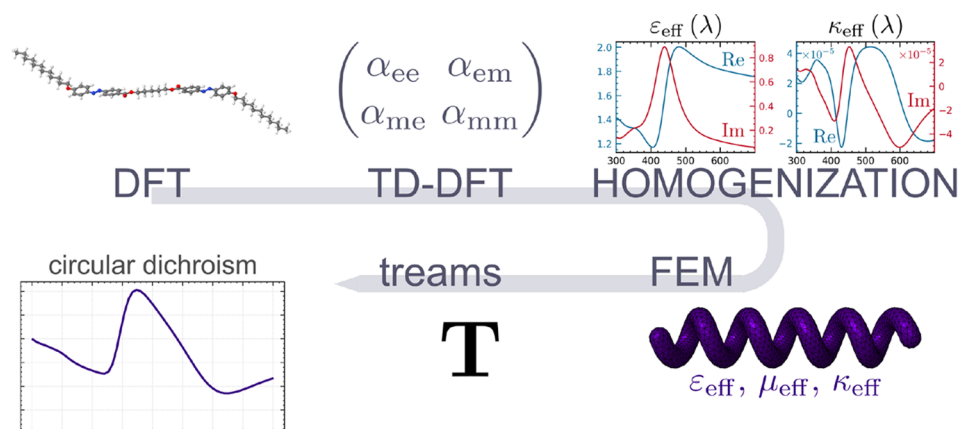
Figure 2. Multiscale modeling workflow for simulating the optical response of helical nanotubes made from organic material. Starting from the structural formula of the molecule, we explore the properties of the single molecule using DFT. We arrive at the chiral molecular geometry (top left) for which the optical properties, i.e., the dynamic polarizabilities α_{ij}, are computed using TD-DFT. According to Lorentz−Lorenz formulas, we then find the parameters characterizing the optical properties of the molecular material ε_{eff}, μ_{eff} and κ_{eff} (top right). The material parameters describe an effective medium consisting of a specified concentration of this molecule. The effective description of the medium, together with a specification of the geometry (bottom right), is then considered in full-wave simulations based on FEM. The linear optical response of an individual helix is extracted in terms of its transition matrix (T-matrix; bottom center). The in-house code `treams` then allows for efficient computations within the T-matrix formalism and extracting quantities of interest, such as the CD (bottom left).
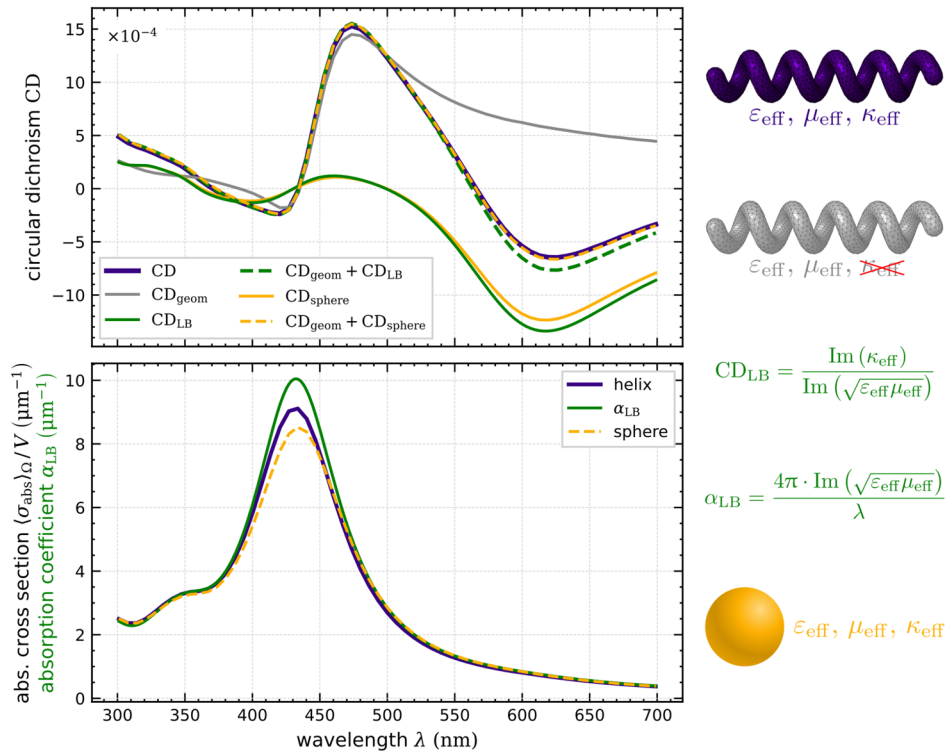
Figure 3. Upper panel: Circular dichroism of a helix made from a chiral medium, described via effective material parameters. The total CD (dark blue) decomposes into a geometry and a material part. The geometrical CD (light gray) is found for the same helix when setting the material chirality parameter to $\kappa_{\mathrm{eff}} = 0$. The material-related CD matches the geometry-independent expression CD_{LB} (green). The superposition (dashed green) of CD_{LB} and the geometrical CD closely matches the total CD of the helix. An even better match is found from the superposition (dashed yellow) of the CD of a sphere with the same volume as the helix (yellow) and the geometrical CD. Lower panel: Absorption cross-section per unit volume and the absorption coefficient for bulk material. The absorption cross-section of the helix (dark blue) is essentially independent of whether the material chirality κ_{eff} is considered or not. A similar absorption spectrum is found for the sphere (dashed yellow). Comparison with the absorption coefficient (green) computed exclusively from the material parameters shows that the material mainly determines the absorption of the considered objects. No significant influence from geometry-related resonances is observed.

object, spanning different length scales. The only input we require is information about the object's geometry and the structural formula of the molecular constituents forming the material from which the object is made. The corresponding results of this approach applied to the example of an organic helix, as depicted in Figure 1, are discussed. The following section then explores the importance of resonances in this context. Afterward, we conclude and give an outlook.

NONRESONANT CASE

In ref 36, the optical response of helical nanotubes forming from an organic thin film of the chiral chemical compound 12OAzo5AzoO12 is studied experimentally. Inspired by these experiments, we have focused our simulations on the optical properties of organic helices. These objects are particularly challenging, as their chirality emerges at two different length scales.

To entirely capture these aspects, we apply a multiscale modeling approach based on refs 37−40. The workflow of this multiscale modeling approach is sketched in Figure 2. Starting from the structural formula of compound 12OAzo5AzoO12, we determine its molecular geometry from density functional theory (DFT) simulations. We found the structure of the chiral molecular geometry shown in Figure 2 at the top left; see also the section Methods. Afterward, time-dependent DFT (TD-DFT), as implemented in the TURBOMOLE quantum chemistry package,[41,42] is applied to calculate the electronic

optical properties and dynamic polarizability tensors of a single molecule in the UV−vis part of the spectrum. Based on the dynamic polarizability, effective material parameters that model a homogeneous, bi-isotropic medium consisting of randomly oriented molecules are derived.[39] Similar to ref 38, we choose a molecular concentration of $c = 3 \times 10^{26}$ m^{-3} to arrive at values of the relative permittivity that appear reasonable for the organic compound.

Accordingly, the organic material will be represented in the following via the three complex-valued scalar parameters, $\varepsilon_{\mathrm{eff}}(\omega)$, $\mu_{\mathrm{eff}}(\omega)$, and $\kappa_{\mathrm{eff}}(\omega)$. They relate the electric and magnetic field strengths and flux densities as described by the common constitutive relations, see Chapter 1 of ref 43.

$$\begin{pmatrix} \dfrac{1}{\varepsilon_0}\mathbf{D}(\mathbf{r}, \omega) \\ c_0\mathbf{B}(\mathbf{r}, \omega) \end{pmatrix} = \begin{pmatrix} \varepsilon_{\mathrm{eff}}(\omega) & \mathrm{i}\kappa_{\mathrm{eff}}(\omega) \\ -\mathrm{i}\kappa_{\mathrm{eff}}(\omega) & \mu_{\mathrm{eff}}(\omega) \end{pmatrix} \begin{pmatrix} \mathbf{E}(\mathbf{r}, \omega) \\ Z_0\mathbf{H}(\mathbf{r}, \omega) \end{pmatrix}.$$

(1)

In the following, the frequency dependence of the material parameters has been omitted for the sake of brevity. Spectra of the effective relative permittivity $\varepsilon_{\mathrm{eff}}$ and the effective material chirality parameter κ_{eff} in the explored wavelength range from 300 to 700 nm are shown on the top right of Figure 2 (a more detailed view is shown in Figure S8 in the Supporting Information (SI)). The effective relative permittivity shows a resonance line shape centered around 440 nm in its imaginary part. This feature relates to the absorption properties of the

molecules and is understood on the level of molecular electronic transitions; see Figures S2 and S3 in the SI, respectively. It leads to substantial absorption by the material in the spectra shown later. We stress that while we also consider the magnetic permeability, its difference from unity is negligible and no notable magnetic response exists.

Upon characterization of the organic material via the effective material parameters, the optical response of an object made from such a material can be computed. Here, the geometric shape is chosen to be a helix with a circular cross-section, as shown in Figure 1. We choose the parameters specifying the geometry with a view to the experimental data in ref 36, namely, a major radius of 41.25 nm, a minor radius of 21.25 nm, and a pitch of 100 nm. The number of turns is set to 5. A corresponding mesh is depicted on the bottom right of Figure 2. The optical response of the object is simulated using the finite element method (FEM) software package JCMsuite[44] and extracted as a transition matrix (T-matrix).[45] This requires simulations of the optical response for a specific set of illuminations and decomposing the scattered field into vector spherical waves. The T-matrix connects the amplitudes of the vector spherical waves that expand the incident field to the amplitudes of the vector spherical waves that expand the scattered field in a matrix-vector product. Using a specific vector spherical wave as the incident field in one simulation, one column of the T-matrix can be extracted. Then, by using a different vector spherical wave in each of these full-wave simulations, the T-matrix is particularly easy to extract.

All relevant experimentally observable quantities can be predicted from the retrieved T-matrix. A prominent example is the absorption cross-section. We use the in-house code treams to compute these quantities of interest.[46] The circular dichroism (CD) is then defined as

$$\text{CD} = \frac{\langle \sigma_{\text{abs}}^+ \rangle_\Omega - \langle \sigma_{\text{abs}}^- \rangle_\Omega}{\langle \sigma_{\text{abs}}^+ \rangle_\Omega + \langle \sigma_{\text{abs}}^- \rangle_\Omega}, \tag{2}$$

where $\langle \cdot \rangle_\Omega$ denotes the orientational average.

Let us now consider the total CD signal of the helix featuring chirality on the geometrical and molecular levels. The total CD signal, as computed from the T-matrix of the helix, is plotted in dark blue in Figure 3. The two scales of chirality of the helix are indicated by the handedness of the helix itself and by the nonzero material chirality parameter κ_{eff}, respectively.

To isolate the effect of the chiral geometry, the CD of a helix with the same geometrical features is computed for $\kappa_{\text{eff}} = 0$. This corresponds to the same geometric object made from an achiral but absorbing material. Since $|\kappa_{\text{eff}}| \ll |\varepsilon_{\text{eff}}|$, the refractive index is not substantially changed by this.

However, the CD signal of such a helix made from an achiral material (shown as the light gray curve in Figure 3) deviates strongly from the previously considered helix made from a chiral material. By construction, this CD signal is exclusively caused by the chiral geometry of the helix. There, the windings determine the phase relation between the helical displacement currents and the induced magnetic field. Combining the absorbing character of the material and a finite volume in a chiral shape, the helix will respond differently to illuminations of different helicity. Due to its purely geometric origin, this CD signal is accordingly called CD_{geom} in the following. Therefore, the difference between CD_{geom} and the total CD discussed

before must be tied to the chirality of the material, i.e., the parameter κ_{eff}.

We want to describe this difference to the overall CD as an individual contribution originating only from the material properties. For this reason, we consider the helicity-dependent absorption found in bulk material, according to the Lambert–Beer law. Here, we find the absorption coefficients

$$\alpha_{\text{LB}}^\pm = 4\pi \cdot \text{Im}(n_\pm)\lambda^{-1}, \tag{3}$$

where $n_\pm = \sqrt{\varepsilon_{\text{eff}}\mu_{\text{eff}}} \pm \kappa_{\text{eff}}$ is the helicity-dependent refractive index. Looking at their relative difference similar to how the CD is evaluated, we define the expression

$$\text{CD}_{\text{LB}} = \frac{\alpha_{\text{LB}}^+ - \alpha_{\text{LB}}^-}{\alpha_{\text{LB}}^+ + \alpha_{\text{LB}}^-} = \frac{\text{Im}(\kappa_{\text{eff}})}{\text{Im}(\sqrt{\varepsilon_{\text{eff}}\mu_{\text{eff}}})}. \tag{4}$$

The subscript LB explicitly refers to the CD evaluated using the Lambert–Beer law for the material. This expression relates a CD signal exclusively to the effective material parameters and is entirely independent of an object's geometry. It is evaluated and presented with the solid green line in Figure 3.

The total CD is closely matched by superimposing the material contribution CD_{LB} onto the isolated geometric contribution CD_{geom}, resulting in the dashed green line. Therefore, in this case, the CD of an object featuring chirality both in its geometry and on the molecular level can be well approximated by a decomposition into a geometry- and a material-related contribution

$$\text{CD} \approx \text{CD}_{\text{geom}} + \text{CD}_{\text{mat}}. \tag{5}$$

The fact that these show marginal interference may be explained by the different length scales on which both origins of chirality are realized. While the geometric chirality is tied to the spatial extent of the object on the order of a few hundred nanometers, the material chirality is substantiated on the molecular level. It stems from the spatially distributed electron density of the molecules.

We have found that a geometry-independent expression describes the material-related CD contribution well. We, therefore, expect that this CD_{mat} also determines the CD found for objects with different shapes that are geometrically achiral and hence do not exhibit a geometric contribution to their CD. To this end, we consider the CD of a sphere, with its volume and material matching that of the helix. This is readily calculated based on analytic solutions for the optical response of a sphere and shown as the solid yellow line in Figure 3. Indeed, it closely matches the purely material-dependent CD_{LB}. However, while the expression CD_{LB} is built from the properties of bulk material, introducing a spatial scale by studying an actual object with a finite volume modifies the obtained CD signal. Yet, since the geometric shape is achiral, $\text{CD}_{\text{sphere}}$ is still caused by the chirality of the material.

Thus, we view the sphere's CD as another manifestation of the material contribution to the CD and study its super-position with the helix's geometrical contribution CD_{geom}. As shown in Figure 3, it excellently matches the total CD of the helix. In fact, this superposition with the material contribution to the CD evaluated in a sphere matches the total CD of the helix even better than that for the entirely geometry-independent term CD_{LB}. We conclude that introducing a spatial scale via a finite absorptive volume affects the material contribution to CD, and that the details of the considered
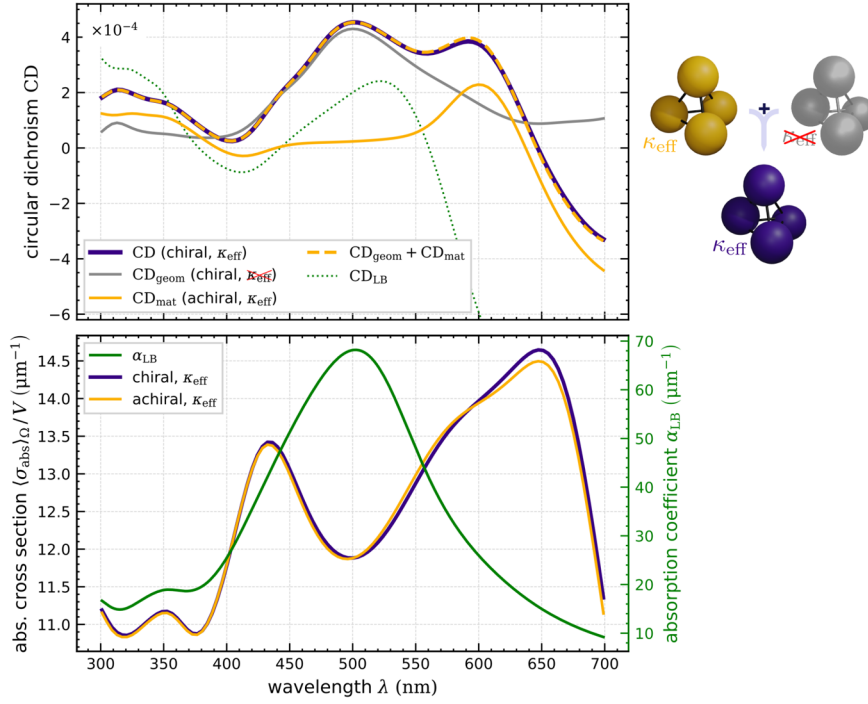
Figure 4. Upper panel: Circular dichroism of tetrahedral arrangements of spheres. A geometry-related CD signal (light gray) is found for the chiral arrangement with the material chirality set to $\kappa_{\text{eff}} = 0$. For the achiral arrangement, the material-related CD (yellow) caused by the nonzero κ_{eff} is found. Due to geometrical resonances, this CD_{mat} differs from the geometry-independent term CD_{LB} (dotted green). The total CD for a chiral arrangement of spheres with nonzero κ_{eff} (dark blue) is again matched by the superposition (dashed yellow) of the isolated geometry- and material-related contributions. Lower panel: Absorption cross-section per unit volume for the tetrahedral arrangements of spheres. The absorption cross-sections exhibit spectral features distinctly different from the absorption coefficient for bulk material (green; right axis). These are due to geometry-related resonances. There are slight differences between the geometrically chiral (dark blue) and achiral (yellow) arrangements, underlining the geometric origin of the spectral features.

geometric shape are virtually irrelevant. This makes sense since all optical resonances of the considered objects appear at much shorter wavelengths. It is then merely the finiteness of the object that affects its optical response. This depends only on the volume of the object independent of the exact shape. It is this subtle interplay between the volume of the object and its optical response that modulates the material contribution to CD.

To evaluate the influence of specifying a geometry on the absorption properties, we look at the absorption spectra of the considered objects. In the bottom panel of Figure 3, the helicity-averaged absorption cross-sections of the helix and the sphere are compared to the absorption coefficient found from the material parameters as

$$\alpha_{\text{LB}} = \frac{1}{2}(\alpha_{\text{LB}}^+ + \alpha_{\text{LB}}^-) = 4\pi \cdot \text{Im}\left(\sqrt{\varepsilon_{\text{eff}}\mu_{\text{eff}}}\right)\lambda^{-1}. \quad (6)$$

The absorption cross-sections of the helix and sphere are normalized to their respective volumes, which are identical. As can be seen from the closely matching curves, the objects' absorption spectra are dominated by the material properties. Specifically, the resonance visible in the imaginary part of ε_{eff} also shows up in the absorption spectra. The line shape is slightly flattened in the absorption cross-sections of the helix and the sphere, revealing the influence of introducing a finite volume.

As a summary of these considerations, we find that the geometrical features of an object shape its absorption profile. This absorption profile, in turn, modulates the material

contribution to the object's CD. This leads to the conclusion that the material contribution, CD_{mat}, of different objects only matches if they show similar absorption spectra.

For the objects examined so far, the absorption spectra were dominated by the absorption characteristic of the material parameters, and hence, they satisfied this condition. In particular, we note that none of them support considerable geometrically induced optical resonances. However, in cases where the absorption spectra of the actual objects are significantly altered from the material's absorption characteristic, i.e., in the presence of geometrically induced resonances, the above consideration should become especially evident. In light of the above, this begs the question of the applicability of our present findings when objects that support substantial resonances are considered.

RESONANT CASE

To address this question, we consider in the following the CD of objects featuring geometrical and material-related chirality while supporting optical resonances. To study the isolated influence of the material chirality, we choose a tetrahedral arrangement of spheres as the starting point. This arrangement is geometrically achiral, and its nonzero CD is, therefore, tied to the chirality of the material from which the spheres are made. By changing the distances between the spheres in the tetrahedral arrangement, we arrive at a geometrically chiral configuration. As we will see below, this causes only a weak perturbation of the absorption spectrum. The geometric chirality of this arrangement, however, causes a CD that can

be evaluated in isolation by considering spheres made from achiral material. The two isolated (geometrical and material) contributions to the CD can then be compared to the combined action of geometric and material-related chirality, which is evaluated for the chiral arrangement of spheres made from chiral material.

To ensure that the individual objects are strongly resonant, we adjust the effective material parameters. These material properties are again computed from the molecular properties of the 12OAzo5AzoO12 dimer. However, this time we consider four times the previous molecular concentration, c = 1.2 × 10^{27} m^{-3}, see Figure S9 in the SI. This causes a strong dispersion in the intrinsic material parameters. The radius of the single sphere is set to r = 80 nm, making the single sphere resonant in the considered spectral range. The achiral tetrahedral arrangement is set up with a center-to-center distance of 220 nm. The chiral arrangement is constructed by lengthening one of the distances between the spheres and shortening one of the distances, each by 20%. The choice of this setup is motivated by the fact that the optical response of a sphere is analytically known. The response of a coupled arrangement of spheres is readily computed using `treams`.

To begin with, the presence of resonances and the comparability of these two arrangements are evaluated again based on the respective absorption spectra in the lower panel of Figure 4. The presence of resonances shows a strong modification of the absorption cross-sections compared to the absorption originating from the material parameters. Yet, both the geometrically chiral and the achiral arrangements exhibit very similar absorption spectra. Slight deviations are explained by the fact that the resonances depend on the coupling between the spheres. Slight changes in the arrangement therefore affect the absorption cross-section.

The CD spectra of the different tetrahedral arrangements of spheres are plotted in the top panel of Figure 4. The total CD of the chiral arrangement featuring a chiral material via a nonvanishing κ_{eff} is again shown in dark blue. The geometrical contribution to the CD is computed by setting κ_{eff} = 0 in this chiral arrangement. To compute the material contribution, the CD of the geometrically achiral arrangement is considered this time with the spheres made from the chiral material. This contribution can be compared to the exclusively material-dependent term CD$_{LB}$. These two results differ substantially, proving the importance of resonances for this analysis. Since resonances are not considered in CD$_{LB}$, the term is not useful for the resonant case.

Having the material- and geometry-related contributions isolated, their superposition can be used to predict the total CD with excellent accuracy. This can be clearly seen in the figure, where the dashed yellow line nearly perfectly agrees with the blue solid line. In general, slight differences can arise due to the differences between the absorption cross-sections for the geometrically chiral and achiral arrangements. It follows that even in the case where the probed objects support optical resonances, the total CD caused by the combined chirality of geometry and material separates into two independent contributions according to CD ≈ CD$_{geom}$ + CD$_{mat}$ to an excellent approximation.

CONCLUSION

The here applied multiscale approach combining precise quantum chemistry simulations of optical properties of molecular materials with Maxwell solvers for photonic objects allowed us to study and understand the origin of the total CD signal for objects and devices that feature both geometry- and material-related chirality. We studied two scenarios and considered cases in which optical resonances supported by the object are present or not. In both cases, we saw that the total CD can be separated into two contributions that are attributed to the geometry- and material-related chirality, respectively.

For nonresonant objects, the material contribution to the CD is virtually identical and independent of the actual geometric details due to their naturally matching absorption spectra, as seen in a comparison between a helix and a sphere of the same volume. This allowed us to analyze the material contribution even without considering any geometry at all. We arrived at an expression for the material contribution to CD that depends only on the material parameters. For resonant objects, the CD remains easily decomposable in cases where an achiral object exists that features the same optical resonances as the chiral object. Therefore, in both cases, the total CD can be written as a sum of a material-dependent contribution (the CD of the geometrically achiral object made from chiral materials) and a geometry-dependent contribution (the CD of the geometrically chiral object made from achiral materials).

The presented analysis promotes a perspective that considers geometry and material as separate originators of the chiral optical response of a given object. This could prove useful both in the computational analysis of chiral objects and in the design of devices relying on the chiral optical properties of their building blocks.

Regarding the former, we may consider that computing the full chiral response of an object featuring material chirality in frequency-domain finite element method simulations, as used here, is computationally expensive. Comparatively, the chiral features attributed purely to the geometry are more readily found in such a setting. Capturing the effect of a nonzero material chirality parameter can render these simulations time-consuming. In contrast, the solely material-dependent CD of a sphere or the entirely geometry-independent expression CD$_{LB}$ introduced in this article are easily evaluated. For a nonresonant system, the total CD could, therefore, also be analyzed by only considering the geometry in full-wave simulations and combining it with the separately and easily computed material contribution. This would save time and computational effort.

Adopting this perspective in the context of the design of optical devices means understanding geometry and material as two independent tunable elements. This offers the prospect of tailoring the chiral response of the object that is defined by the combination of those two elements. As an exemplary scenario, it would be interesting to explore the possibilities of arriving at a chosen chiral response, such as a broad, near-constant CD signal, for a given chiral material by designing the geometry accordingly.

A preprint of this article is available at DOI: 10.48550/arXiv.2401.06664.[47]

METHODS

The multiscale approach employed in this work spans the scales from molecular materials to microscopic object sizes, employing the T-matrices as the bridge. T-matrices are calculated from damped dynamic polarizabilities on the quantum level using the development version of the TURBOMOLE 7.7 program package for electronic structure

calculations using density functional theory.[41] Thus, we first start by looking into the structure of the single 12OAzo5A-zoO12 molecule by geometry optimization in vacuum. We combined generalized-gradient approximation PBE exchange-correlation functional[48,49] with Karlsruhe def2-TZVP basis set[50,51] and Grimme's D4 dispersion correction[52,53] to obtain both chiral and achiral structure of the single molecular building block of the helix (Figure S1). Resolution-of-identity (RI)[54,55] and multipole-accelerated resolution-of-identity[56] algorithms were applied to speed up the calculations without influencing the quality of the final results. To confirm that the obtained structures are the local minima on the potential energy surface of the ground state, we performed a molecular vibrational analysis. All vibrational modes had real frequencies, indicating that we found a stable configuration. Both chiral and achiral molecules have the same total energy, rendering them energetically degenerate conformers. Before tackling the calculations of the dynamic polarizabilities, we need to determine the spectral range where electronic excitations for both absorption and circular dichroism of this molecule happen. In that context, the standard approach to calculate the absorption spectra and rotatory strengths for both conformers was applied. The complete analysis of those optical properties is given in the Supporting Information, Figures S2–S7, and it is not discussed here in detail.

We then proceeded to calculate the electric-electric, electric-magnetic, and magnetic-magnetic dynamic polarizability tensors later used to construct T-matrices and perform homogenization of the effective material parameters. Polarizability tensors were produced for the spectral window from 300 to 700 nm with a wavelength resolution of 1 nm. We obtained the complex values of the polarizability elements by applying a constant damping factor of 0.1 eV for the entire spectral range. Both chiral and achiral conformers exhibited the same absorption spectrum, while only a chiral version had a CD absorption signal, as expected. The complete set of DFT and TD-DFT calculations is archived in NOMAD database under the following DOI: 10.17172/NOMAD/2023.12.22-2.

AUTHOR INFORMATION

Corresponding Author

Lukas Rebholz − *Institute of Theoretical Solid State Physics, Karlsruhe Institute of Technology, 76131 Karlsruhe, Germany;* orcid.org/0009-0001-0737-7826; Email: lukas.rebholz@kit.edu

Authors

Marjan Krstić − *Institute of Theoretical Solid State Physics, Karlsruhe Institute of Technology, 76131 Karlsruhe, Germany;* orcid.org/0000-0002-9484-3396

Benedikt Zerulla − *Institute of Nanotechnology, Karlsruhe Institute of Technology, 76131 Karlsruhe, Germany;* orcid.org/0000-0002-8173-3761

Mateusz Pawlak − *Faculty of Chemistry, University of Warsaw, 02-093 Warsaw, Poland;* orcid.org/0000-0002-4487-7504

Wiktor Lewandowski − *Faculty of Chemistry, University of Warsaw, 02-093 Warsaw, Poland*

Ivan Fernandez-Corbaton − *Institute of Nanotechnology, Karlsruhe Institute of Technology, 76131 Karlsruhe, Germany;* orcid.org/0000-0003-2834-5572

Carsten Rockstuhl − *Institute of Theoretical Solid State Physics, Karlsruhe Institute of Technology, 76131 Karlsruhe, Germany; Institute of Nanotechnology, Karlsruhe Institute of Technology, 76131 Karlsruhe, Germany*

REFERENCES

(1) Schäferling, M. *Chiral Nanophotonics*; Springer Series in Optical Sciences; Springer: Cham, 2017; Vol. *205*.

(2) Wang, B.; Zhou, J.; Koschny, T.; Kafesaki, M.; Soukoulis, C. M. Chiral metamaterials: simulations and experiments. *Journal of Optics A: Pure and Applied Optics* **2009**, *11*, 114003.

(3) Baranov, D. G.; Schäfer, C.; Gorkunov, M. V. Toward Molecular Chiral Polaritons. *ACS Photonics* **2023**, *10*, 2440−2455.

(4) Woody, R. W. Biochemical Spectroscopy. *Methods in Enzymology*; Academic Press, 1995; Vol. *246*, pp 34−71.

(5) Wang, X.; Tang, Z. Circular Dichroism Studies on Plasmonic Nanostructures. *Small* **2017**, *13*, 1601115.

(6) Solomon, M. L.; Saleh, A. A. E.; Poulikakos, L. V.; Abendroth, J. M.; Tadesse, L. F.; Dionne, J. A. Nanophotonic Platforms for Chiral Sensing and Separation. *Acc. Chem. Res.* **2020**, *53*, 588−598.

(7) Warning, L. A.; Miandashti, A. R.; McCarthy, L. A.; Zhang, Q.; Landes, C. F.; Link, S. Nanophotonic Approaches for Chirality Sensing. *ACS Nano* **2021**, *15*, 15538−15566.

(8) Vázquez-Lozano, J. E.; Martínez, A. Toward Chiral Sensing and Spectroscopy Enabled by All-Dielectric Integrated Photonic Waveguides. *Laser & Photonics Reviews* **2020**, *14*, 1900422.

(9) García-Guirado, J.; Svedendahl, M.; Puigdollers, J.; Quidant, R. Enhanced Chiral Sensing with Dielectric Nanoresonators. *Nano Lett.* **2020**, *20*, 585−591.

(10) Olmos-Trigo, J.; Sugimoto, H.; Fujii, M. Far-Field Detection of Near-Field Circular Dichroism Enhancements Induced by a Nanoantenna. *Laser & Photonics Reviews* **2024**, 2300948.

(11) Zhou, S.; Bian, J.; Chen, P.; Xie, M.; Chao, J.; Hu, W.; Lu, Y.; Zhang, W. Polarization-dispersive imaging spectrometer for scattering circular dichroism spectroscopy of single chiral nanostructures. *Light: Science & Applications* **2022**, *11*, 64.

(12) Hu, H.; Gan, Q.; Zhan, Q. Generation of a Nondiffracting Superchiral Optical Needle for Circular Dichroism Imaging of Sparse Subdiffraction Objects. *Phys. Rev. Lett.* **2019**, *122*, 223901.

(13) Milton, F. P.; Govan, J.; Mukhina, M. V.; Gun'ko, Y. K. The chiral nano-world: chiroptically active quantum nanostructures. *Nanoscale Horiz* **2016**, *1*, 14−26.

(14) Hentschel, M.; Schäferling, M.; Duan, X.; Giessen, H.; Liu, N. Chiral plasmonics. *Science Advances* **2017**, *3*, No. e1602735.

(15) Collins, J. T.; Kuppe, C.; Hooper, D. C.; Sibilia, C.; Centini, M.; Valev, V. K. Chirality and Chiroptical Effects in Metal Nanostructures: Fundamentals and Current Trends. *Advanced Optical Materials* **2017**, *5*, 1700182.

(16) Valev, V. K.; Baumberg, J. J.; Sibilia, C.; Verbiest, T. Chirality and Chiroptical Effects in Plasmonic Nanostructures: Fundamentals, Recent Progress, and Outlook. *Adv. Mater.* **2013**, *25*, 2517−2534.

(17) Schäferling, M.; Dregely, D.; Hentschel, M.; Giessen, H. Tailoring Enhanced Optical Chirality: Design Principles for Chiral Plasmonic Nanostructures. *Phys. Rev. X* **2012**, *2*, 031010.

(18) MacKay, T. G.; Lakhtakia, A. *Electromagnetic Anisotropy And Bianisotropy: A Field Guide*; World Scientific Publishing, 2010.

(19) Sihvola, A. H.; Lindell, I. V. BI-isotropic constitutive relations. *Microwave and Optical Technology Letters* **1991**, *4*, 295−297.

(20) Engheta, N.; Jaggard, D. L. Electromagnetic chirality and its applications. *IEEE Antennas and Propagation Society Newsletter* **1988**, *30*, 6−12.

(21) Quack, M. Structure and Dynamics of Chiral Molecules. *Angewandte Chemie International Edition in English* **1989**, *28*, 571−586.

(22) Höflich, K.; Feichtner, T.; Hansjürgen, E.; Haverkamp, C.; Kollmann, H.; Lienau, C.; Silies, M. Resonant behavior of a single plasmonic helix. *Optica* **2019**, *6*, 1098−1105.

(23) Woźniak, P.; De Leon, I.; Höflich, K.; Leuchs, G.; Banzer, P. Interaction of light carrying orbital angular momentum with a chiral dipolar scatterer. *Optica* **2019**, *6*, 961−965.

(24) Lingstädt, R.; Davoodi, F.; Elibol, K.; Taleb, M.; Kwon, H.; Fischer, P.; Talebi, N.; van Aken, P. A. Electron Beam Induced Circularly Polarized Light Emission of Chiral Gold Nanohelices. *ACS Nano* **2023**, *17*, 25496.

(25) Zhang, X.; Xu, Y.; Valenzuela, C.; Zhang, X.; Wang, L.; Feng, W.; Li, Q. Liquid crystal-templated chiral nanomaterials: from chiral plasmonics to circularly polarized luminescence. *Light: Science & Applications* **2022**, *11*, 223.

(26) Kotov, N. A.; Liz-Marzán, L. M.; Wang, Q. Chiral nanomaterials: evolving rapidly from concepts to applications. *Mater. Adv.* **2022**, *3*, 3677−3679.

(27) Albano, G.; Pescitelli, G.; Di Bari, L. Chiroptical Properties in Thin Films of π-Conjugated Systems. *Chem. Rev.* **2020**, *120*, 10145−10243.

(28) Yang, Y.; da Costa, R. C.; Smilgies, D.-M.; Campbell, A. J.; Fuchter, M. J. Induction of Circularly Polarized Electroluminescence from an Achiral Light-Emitting Polymer via a Chiral Small-Molecule Dopant. *Adv. Mater.* **2013**, *25*, 2624−2628.

(29) Zhai, D.; Jiang, J.; Yuan, C.; Wang, D.; Jiang, Y.; Liu, M. Fluorescence Filter Nanoarchitectonics with Polydiacetylene-Based Supramolecular Chiral Gel for Generating Tunable Circularly Polarized Luminescence. *Advanced Optical Materials* **2023**, *11*, 2300161.

(30) Park, W.; Ha, T.; Kim, T.-T.; Zep, A.; Ahn, H.; Shin, T. J.; Sim, K. I.; Jung, T. S.; Kim, J. H.; Pociecha, D.; Gorecka, E.; Yoon, D. K. Directed self-assembly of a helical nanofilament liquid crystal phase for use as structural color reflectors. *NPG Asia Materials* **2019**, *11*, 45.

(31) Wade, J.; et al. Natural optical activity as the origin of the large chiroptical properties in π-conjugated polymer thin films. *Nat. Commun.* **2020**, *11*, 6137.

(32) Both, S.; Schäferling, M.; Sterl, F.; Muljarov, E. A.; Giessen, H.; Weiss, T. Nanophotonic Chiral Sensing: How Does It Actually Work? *ACS Nano* **2022**, *16*, 2822−2832.

(33) Tkachenko, G.; Brasselet, E. Optofluidic sorting of material chirality by chiral light. *Nat. Commun.* **2014**, *5*, 3577.

(34) Casida, M. E. Time-dependent density-functional theory for molecules and molecular solids. *Journal of Molecular Structure: THEOCHEM* **2009**, *914*, 3−18.

(35) Lavrinenko, A. V.; Lægsgaard, J.; Gregersen, N.; Schmidt, F.; Søndergaard, T. *Numerical Methods in Photonics*; CRC Press, 2018.

(36) Jedrych, M.; Pawlak, M.; Gorecka, E.; Lewandowski, W.; Wojcik, M. M. Light-Responsive Supramolecular Nanotubes-Based Chiral Plasmonic Assemblies. *ACS Nano* **2023**, *17*, 5548−5560.

(37) Fernandez-Corbaton, I.; Beutel, D.; Rockstuhl, C.; Pausch, A.; Klopper, W. Computation of electromagnetic properties of molecular ensembles. *ChemPhysChem* **2020**, *21*, 878−887.

(38) Zerulla, B.; Krstić, M.; Beutel, D.; Holzer, C.; Wöll, C.; Rockstuhl, C.; Fernandez-Corbaton, I. A multi-scale approach for modeling the optical response of molecular materials inside cavities. *Adv. Mater.* **2022**, *34*, 2200350.

(39) Zerulla, B.; Venkitakrishnan, R.; Beutel, D.; Krstić, M.; Holzer, C.; Rockstuhl, C.; Fernandez-Corbaton, I. A T-Matrix Based Approach to Homogenize Artificial Materials. *Advanced Optical Materials* **2023**, *11*, 2201564.

(40) Zerulla, B.; Li, C.; Beutel, D.; Oßwald, S.; Holzer, C.; Bürck, J.; Bräse, S.; Wöll, C.; Fernandez-Corbaton, I.; Heinke, L.; Rockstuhl, C.; Krstić, M. Exploring Functional Photonic Devices made from a Chiral Metal−Organic Framework Material by a Multiscale Computational Method. *Adv. Funct. Mater.* **2023**, 2301093.

(41) Turbomole 7.7. 2022; https://www.turbomole.org.

(42) Franzke, Y. J.; et al. TURBOMOLE: Today and Tomorrow. *J. Chem. Theory Comput.* **2023**, *19*, 6859.

(43) Kristensson, G. *Scattering of Electromagnetic Waves by Obstacles*; SciTech Publishing, 2016.

(44) JCMsuite 5.4.0. 2022; https://jcmwave.com/jcmsuite.

(45) Waterman, P. C. Matrix formulation of electromagnetic scattering. *Proc. IEEE* **1965**, *53*, 805−812.

(46) Beutel, D.; Fernandez-Corbaton, I.; Rockstuhl, C. treams − a T-matrix-based scattering code for nanophotonics. *Comput. Phys. Commun.* **2024**, *297*, 109076.

(47) Rebholz, L.; Krstić, M.; Zerulla, B.; Pawlak, M.; Lewandowski, W.; Fernandez-Corbaton, I.; Rockstuhl, C. Separating the Material and Geometry Contribution to the Circular Dichroism of Chiral Objects Made from Chiral Media. *arXiv:2401.06664 [physics.optics]* **2024**, na.

(48) Perdew, J. P.; Burke, K.; Ernzerhof, M. Generalized Gradient Approximation Made Simple. *Phys. Rev. Lett.* **1996**, *77*, 3865−3868.

(49) Perdew, J. P.; Burke, K.; Ernzerhof, M. Generalized Gradient Approximation Made Simple. *Phys. Rev. Lett.* **1996**, *77*, No. 3865.

(50) Weigend, F.; Ahlrichs, R. Balanced Basis Sets of Split Valence, Triple Zeta Valence and Quadruple Zeta Valence Quality for H to Rn: Design and Assessment of Accuracy. *Phys. Chem. Chem. Phys.* **2005**, *7*, 3297−3305.

(51) Weigend, F. Accurate Coulomb-fitting Basis Sets for H to Rn. *Phys. Chem. Chem. Phys.* **2006**, *8*, 1057−1065.

(52) Caldeweyher, E.; Bannwarth, C.; Grimme, S. Extension of the D3 Dispersion Coefficient Model. *J. Chem. Phys.* **2017**, *147*, 034112.

(53) Caldeweyher, E.; Ehlert, S.; Hansen, A.; Neugebauer, H.; Spicher, S.; Bannwarth, C.; Grimme, S. A Generally Applicable Atomic-Charge Dependent London Dispersion Correction. *J. Chem. Phys.* **2019**, *150*, 154122.

(54) Eichkorn, K.; Treutler, O.; Öhm, H.; Häser, M.; Ahlrichs, R. Auxiliary Basis Sets to Approximate Coulomb Potentials. *Chem. Phys. Lett.* **1995**, *240*, 283−290.

(55) Eichkorn, K.; Weigend, F.; Treutler, O.; Ahlrichs, R. Auxiliary Basis Sets for Main Row Atoms and Transition Metals and Their Use to Approximate Coulomb Potentials. *Theor Chem. Acta* **1997**, *97*, 119−124.

(56) Sierka, M.; Hogekamp, A.; Ahlrichs, R. Fast Evaluation of the Coulomb Potential for Electron Densities Using Multipole Accelerated Resolution of Identity Approximation. *J. Chem. Phys.* **2003**, *118*, 9136−9148.